Limnol. Oceanogr., 50(1), 2005, 207–216

Internal seiche dynamics in Lake Geneva

U. Lemmin[1]
Swiss Federal Institute of Technology, Laboratory of Environmental Hydraulics, CH-1015 Lausanne, Switzerland

C. H. Mortimer
Center for Great Lakes Studies, University of Wisconsin-Milwaukee, Milwaukee, Wisconsin 53204

E. Bäuerle
University of Constance, Department of Biology, D-78457 Constance, Germany

Abstract

We analyzed season-long water level records at 12 stations around the Lake of Geneva (local name Léman) for evidence of internal seiches modified by Coriolis force and compared the results with predictions from a two-layer numerical model with real bottom topography for typical wind situations. Results are also compared with those obtained from current and temperature measurements in the lake. Agreement was satisfactory in all cases. Model predictions and measurements both indicated that only three internal seiche modes are excited: the 1st mode and the 3rd mode, which are Kelvin-seiche oscillations, and the 12th mode, which is a Poincaré seiche. The model, driven by winds from different directions, demonstrates that the wind field, constrained by the local topography, determines which of the modes is generated.

Long internal waves in lakes commonly take the form of standing waves (seiches) of frequency and structure determined by basin shape and density (temperature) stratification in the water column (Wedderburn 1912; Mortimer 1953). The history of research on such waves is reviewed by Mortimer (1993); and their rotation-affected roles in a large lake (Lake Michigan) are described in Mortimer (2004).

A controlling length scale is the Rossby radius of deformation, $a = c_i/f$, in which f is the latitude-dependent Coriolis parameter and c_i is the speed of long, internal waves in the absence of rotation. When the basin rotates and its width exceeds a, the waves take the form of amphidromic internal seiche modes. As described below, the first horizontal mode resembles a shore-hugging wave of a form similar to a Kelvin wave (Platzman 1971) traveling counterclockwise (cyclonically) around the lake basin in northern hemisphere lakes, as was first demonstrated in the Lake of Geneva by Mortimer (1963) and later in Lake Biwa, Japan, by Kanari (1975, 1984). We will use the term Kelvin seiche for this wave in the present text.

Records of Lake Geneva currents and/or thermocline-depth oscillations during the stratified season (Bohle-Carbonell 1986) occasionally revealed one or two whole-basin circuits of shore-hugging internal Kelvin waves during calm intervals following storms. Bohle-Carbonell and van Senden (1990) viewed those responses as too ephemeral and incoherent to be interpreted as whole-basin modes. They therefore concluded that currents in large lakes, at least those in Lake Geneva, may be best described as transient in time and only locally organized in space. Although those responses are often short-lived, our results clearly identify them as whole-basin internal seiche modes excited by wind action, either singly or in combination.

It should be noted that the thermocline oscillations are accompanied by oscillations at lake-surface level, which are out-of-phase with and typically about 1/1,000 smaller in amplitude than the oscillations of thermocline isotherms. It is therefore possible (e.g., Caloi et al. 1961; Sirkes 1987) to use filtered deviations of surface level from equilibrium to follow the progress of internal motions. Here we apply this method to study internal wave dynamics in the Lake of Geneva using data from 12 high-precision water-level recorders spaced around the lake shore by the Swiss Service Fédérale des Eaux, (SFE; 1954) in 1950 (Fig. 1).

Mortimer (1963) had plotted the SFE surface levels in cyclonic order around the basin for eight stations. Following an initiating wind impulse, the nearly constant counterclockwise progression of two cycles of an 80-h wave, with a speed of progress close to $c_i \approx 45$ cm s^{-1}, was made evident. The internal wave speed c_i was consistent with a basin width of about $2a$. The remarkably close correlation between the level record at Sécheron (station 1 in Fig. 1) and the temperature at the 15-m deep nearby Geneva water intake supported the hypothesis that this wave was the surface signal of a much larger thermocline wave (amplitude of order ± 5 m).

For higher horizontal modes, the resulting rotating internal wave patterns in large lakes depend on the basin shape and size and become more complicated. Observations are lacking. The spatial structure of higher modes can best be visualized through comparisons of numerical model results with observations. In the present study, we will use the SFE

[1] Corresponding author (ulrich.lemmin@epfl.ch).

Acknowledgments

The limnograph data were made available by the Service Fédéral des Eaux (SFE) of Switzerland. Part of the analysis was carried out within the framework of the project EUROLAKES (EU contract EVK1-CT1999-00004) sponsored by the Swiss Federal Office of Science and Research (contract 99.0190). We are grateful for the support. We would like to thank S. A. Thorpe and two reviewers for their careful reading and their suggestions for improvement.

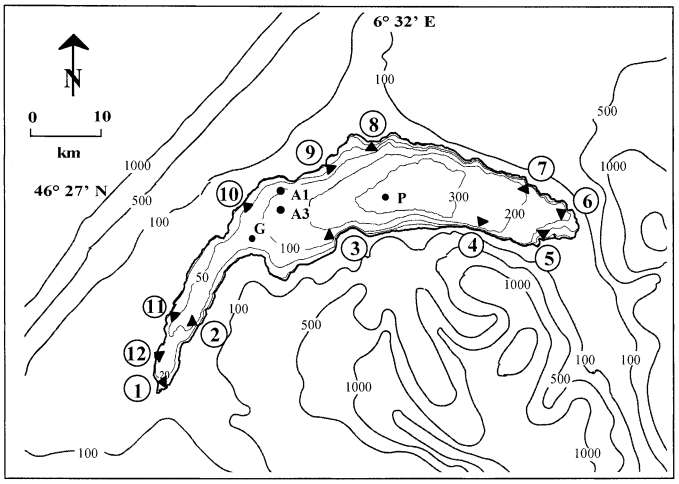

Fig. 1. Map of the Lake of Geneva (Léman) with surrounding topography and positions of water-level recording stations. Elevation of surrounding land and depths within the lake are given in meters with respect to the water surface of the lake. Also indicated are the positions of mooring stations within the lake. For details, see text.

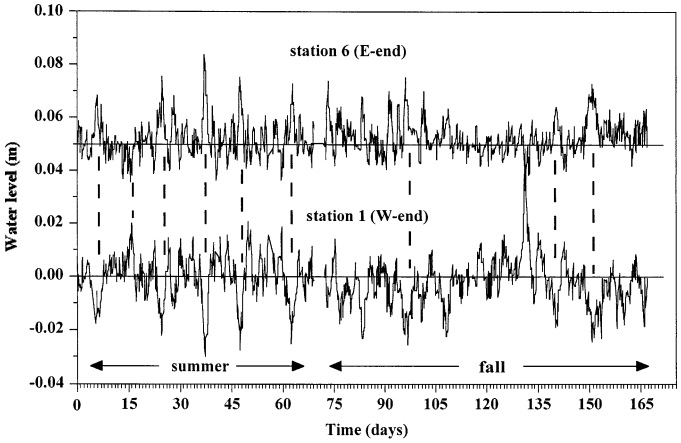

Fig. 2. SFE smoothed water-level records at stations 1 (west end) and 6 (east end). The mean trends have been removed. The level of station 6 has been shifted upward by 0.05 m for clarity. Dashed vertical lines indicate some events during which strong level excursions with opposite sign have been identified at the opposite ends of the lake.

(1954) surface-level data to first compare observations and model results for the first-mode Kelvin seiche and then explore higher modes.

The Lake of Geneva environment—The Lake of Geneva (Fig. 1) is a warm monomictic lake. It is composed of two basins: a deep central eastern basin (310 m maximum depth, 157 m mean depth, mean width 10 km) and a relatively small and narrow section in the west (maximum depth 70 m, mean width about 4 km). The lake has a total length of 70.2 km and a width of 13.8 km in the central part, which corresponds to 2.4 Rossby radii under typical summer stratification conditions.

The wind field over the lake is affected by the topography (Lemmin and D'Adamo 1996): The eastern part of the lake, surrounded by high mountains, is sheltered from most strong winds. Over the central and western part of the lake, it is dominated by randomly occurring events of strong winds from the northeast and southwest, which may last from several hours to several days. The winds from the northeast have been observed to cause thermocline depressions of more than 20 m in the western part (Lemmin and D'Adamo 1996).

Data and methods

Water level data—From the recorded water levels (4 June–30 November 1950), 6-h mean levels were tabulated by the SFE at 3-h intervals, thereby filtering out level fluctuations of 3-h periods or less (i.e., surface seiches, Forel 1895; for details, see SFE 1954). For the present analysis, occasionally missing points were replaced by linear interpolation over five or six surrounding points. In the following analysis, the SFE data set was divided into a summer period from 4 June to 24 August and a fall period from 28 August to 30 November.

Changes in mean lake water levels have been eliminated by subtracting the corresponding 12-station mean value from each observation. The effect of wind setup is more difficult to eliminate because wind-forcing events occur on timescales of hours to several days, which fall into the period range of the internal seiches to be analyzed. Setup effects, arising from short wind events, are reduced by the SFE filter. No objective method for the elimination of setup effects of wind events lasting a day or so from every station can be devised. Also unknown is the influence on setup of local topographic sheltering by surrounding mountains.

Typical examples of the smoothed water-level time series are illustrated in Fig. 2 for stations at the east (station 6) and west (station 1) ends of the basin. A systematic out-of-phase behavior of the large-amplitude excursions can be seen. Thus, even though strong wind forcing mainly acts over the western and central part of the lake, the lake at the eastern end still responds as though forcing had occurred along the whole of the lake axis.

Data analysis techniques—For spectral analysis of records, such as those illustrated in Fig. 2, a standard fast Fourier transform with segment overlap was used. Analysis for all stations was carried out separately for the summer and fall periods. Cross-spectral analysis, applied to station pairs, was used to determine interstation coherence and phase. These were compared with the spatial structures of seiche modes, simulated by the two-layer, real topography numerical model described below.

Numerical model—In order to gain insight into the response of the Lake of Geneva to realistic winds during summer and autumn, we investigated the hydrodynamics of the lake with the bottom topography as shown in Fig. 1 on the rotating Earth (*f*-plane). We carried out the investigations in the time domain and in the frequency domain.

A reasonable approximation of the vertical stratification

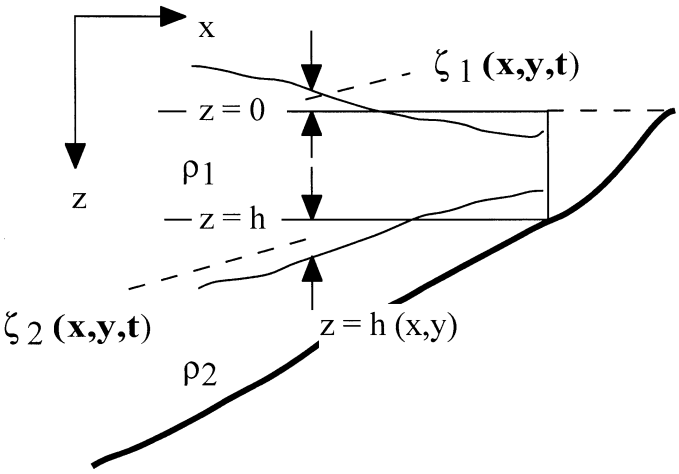

Fig. 3. Definition sketch for a two-layer water column of variable depth.

in summer and autumn is given by two layers of water with slightly different densities. A two-layer representation, as adopted in the model, confines its application to the study of only the first vertical mode.

Assuming that the motion in each layer is independent of depth, and using the notation shown in Fig. 3, the linearized equations without friction between the layers are

for the upper layer (h_1 = constant)

$$\frac{\partial V_1}{\partial t} + fk \times V_1 = gh_1\nabla\zeta_1 + \frac{\tau_w}{\rho_1} \tag{1}$$

$$\nabla\cdot V_1 + \frac{\partial\zeta_1}{\partial t} - \frac{\partial\zeta_2}{\partial t} = 0 \tag{2}$$

for the lower layer [$h_2 = h_2(x, y)$]

$$\frac{\partial V_2}{\partial t} + fk \times V_2 = -g\delta h_2\nabla\zeta_1 - g\varepsilon h_2\nabla\zeta_2 - \frac{\tau_B}{\rho_2} \tag{3}$$

$$\nabla\cdot V_2 + \frac{\partial\zeta_2}{\partial t} = 0 \tag{4}$$

The vectors of horizontal transport in the layers are $V_i = (U_i, V_i)$ (i = 1, 2). ζ_i are the vertical displacements of the surface (i = 1) and of the thermocline (i = 2), and $\delta \equiv \rho_1/\rho_2$, $\varepsilon = (\rho_2 - \rho_1)/\rho_2$. The wind stress, τ_w, at the surface is assumed to be known and the stress at the bottom of the basin must be expressed in terms of the flow field. Furthermore, we assume that there is no momentum or mass transfer across the interface. At the shoreline, the condition of zero mass transport normal to the lateral boundaries has to be fulfilled.

For the undamped free modes of oscillation during summer stratification in the Lake of Geneva, we obtain the free oscillations of the system by assuming that the variables have a simple harmonic dependence on time of the form $e^{i\omega t}$, where ω is the frequency of oscillation,

$$(V_i, \zeta_i) = (\mathbf{Q_i}, Z_i)e^{i\omega t} \tag{5}$$

Here, $\mathbf{Q_i} = (M_i, N_i)$ are the complex amplitudes of the horizontal components of transport in the respective layers and Z_i are the complex amplitudes of the displacements of the surface and the interface. The equations can then be converted into an eigenvalue problem, which may be written as

$$i\omega\mathbf{a} + \Re\mathbf{a} = 0 \tag{6}$$

where

$$\mathbf{a} \equiv \begin{pmatrix}\mathbf{Q}_1\\ Z_1\\ \mathbf{Q}_2\\ Z_2\end{pmatrix}, \qquad \Re \equiv \begin{pmatrix} fk\times & gh_1\nabla & 0 & 0\\ \nabla\cdot & 0 & \nabla\cdot & 0\\ 0 & g\delta h_2\nabla & fk\times & g\varepsilon h_2\nabla\\ 0 & 0 & \nabla\cdot & 0\end{pmatrix} \tag{7}$$

The characteristic values ω_n (n = 1, 2, . . .) of the operator $\Re$ in (7) represent the frequencies of free oscillation, and the $\mathbf{a}_n$ are the corresponding eigenvectors. Each eigenvector $\mathbf{a}_n$ is a function of the horizontal coordinates and represents the spatial structure of a normal mode associated with a particular frequency, ω_n.

In order to discretize the problem in the horizontal directions, a rectangular grid with a mesh size of 500 m × 500 m was used to cover the lake's surface. The grid of the eigenfrequency model was identical to the one used by Bäuerle (1985). The numerical grid of the time-stepping model is formed by ζ-points, which are placed centrally between points where the components of the horizontal volume transports are evaluated (U—points in the x-direction, V—points in y-direction, respectively). Horizontal discretization in both models is done by central differences. Time stepping is done by an alternate direction implicit (ADI) procedure with the Coriolis term resulting from averaging of the surrounding U-components at the grid-point where V is computed, and vice versa. Wind stress is represented by a force driving the entire upper layer.

Depending on stratification, the following assumptions concerning the horizontal extent of the lake have been made: In the calculation of the response during the summer and autumn stratification, respectively, we introduce vertical walls down to the intersection of the thermocline with the bottom. The resulting depth contour is defined as the boundary of the stratified lake, thus ignoring the influence of the shallow parts of the lake with only epilimnic water. Consequently, the lateral boundaries of the model differ slightly between the seasons due to the deeper lying autumnal thermocline.

In the model calculations we assumed, for the summer (values in parentheses for the fall) a top layer h_1 = 15 (25) m; a bottom layer h_2 = 175 (165) m; a top-layer temperature T_1 = 19 (8)°C; and a bottom-layer temperature T_2 = 5.5°C. The maximum wind velocity for the forcing is always taken as 5 m s^{-1}. The thermocline excursions predicted by the time-stepping model are given in meters. However, no verification with measured data was possible. The amplitudes of the excursions should therefore be considered as relative to this forcing. The free modes of oscillation, which result from the solution of the eigenvalue problem expressed by Eq. (6) with the boundary conditions, are found to be in perfect agreement with the corresponding results of the time-stepping model.

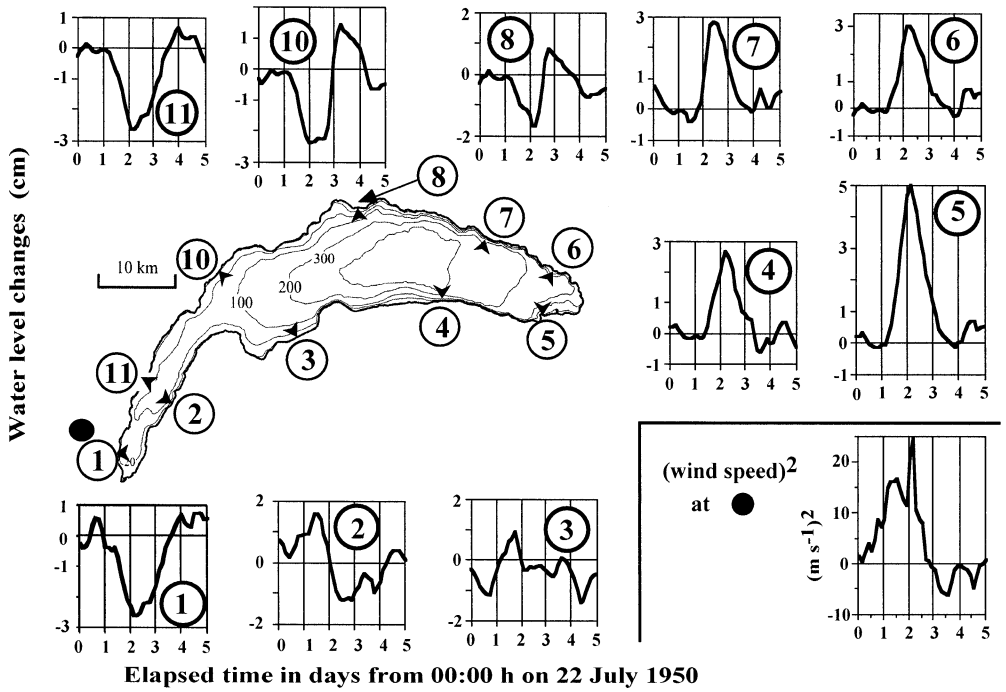

Fig. 4. Response of the water level around the lake to an episode of southwest wind starting at 0000 h on 22 July 1950. Wind is shown (at bottom right) as speed squared of the component directed 40° east of north, which peaked at 5 m s^{-1} (18 km h^{-1}) 2 days and 6 h from the start.

Comparison of data analysis and numerical modeling for mode detection

The present section explores wave modes by (i) spectral analysis of the SFE surface level records; and (ii) by numerical simulation in a topographically realistic basin. In this investigation, modes were identified by comparing the periods corresponding to prominent spectral peaks from the data analysis with the predominant structures revealed by the numerical model.

Surface-level data—The wavelike response is investigated here by plotting the pattern of the SFE surface excursions around the basin during a typical forcing event (Fig. 4). Three different conclusions emerge:

1. As soon as a strong and steady wind from the southwest sets in, the whole lake responds by a depression at the west end (stations 1, 12) and a rise at the east end (stations 4, 5, and 6). The rise at station 5 was always found to be significantly higher than at stations 4 or 6. This may be attributed to a combination of wind-induced surface elevation with the inflow of the Rhone river (± 200 m^3 s^{-1}), which enters the lake close to station 5. In the case of forcing from the opposite direction, the depression at station 5 is comparable with those at stations 4 and 6, but the elevation at stations 1 and 12 at the narrow west end becomes very pronounced, being about four times as high as the depression at the wide east end.

2. During the initial phase of the forcing, geostrophic adjustment is revealed by a slight rise in level at stations 2 and 3 and a fall in level at stations 10 and 11. This effect of the Coriolis force was also found in all other wind-forced events investigated.

3. During the first half of day 2, the wind event died down rapidly. It can be seen (Fig. 4) that the corresponding lake-level changes occurred at a much slower rate. Furthermore, a cyclonic pattern was set in motion at the east end of the lake. The appearance of the peak of maximum elevation in the records of stations 6–11 was systematically shifted in time and occurred at station 10 a full day after station 6. This pattern continued into the western basin with a reduced amplitude at station 11.

A similar picture was also observed during other events. Rises in surface level correspond to thermocline depressions. As will be shown later, evidence for internal Kelvin seiches in current and temperature measurements in the water column are always related to thermocline depressions. It can thus be seen from the surface-elevation data in Fig. 4 that Kelvin seiches are set in motion at the east end of the lake in the case of wind forcing from the southwest, even though that end is not under direct influence of the wind. This is different from forcing by northeastern wind, when the west end is directly affected by the wind. The high surface elevations, observed in this case, cause strong depression of the thermocline at the west end.

Spectral analysis revealed that independent of season and station location, only certain modes were excited. The most prominent is the first (L1) mode (Fig. 5). Its period is near 81.5 h in summer, increasing to above 130 h in fall, as the density structure of the water column changes and c_i decreases. Spectra from the narrow western end of the lake always showed the L1 mode response most clearly. A weak

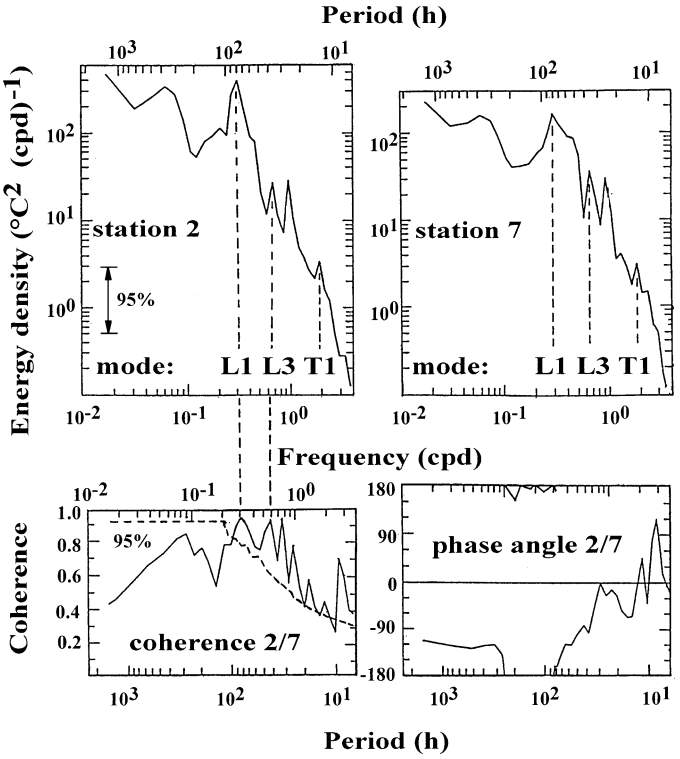

Fig. 5. Top: spectra of SFE water-level fluctuations at stations 2 and 7 during the summer interval 4 June–24 August 1950. Bottom: coherence and phase angle between stations 2 and 7.

second mode (L2) signal could be detected in the spectra of some stations in the central part of the lake (stations 3 and 8), but not at other stations. The L3 mode, with periods of 33.3 h and near 50 h during summer and fall, respectively, was found at all stations around the lake. A weak mode L4 seiche was found in some summer spectra but not in those for the fall. Modes L5–L9 were not observed in any spectra. Mode L10 is interpreted as the first cross basin or transverse mode with summer and fall periods of 10.7 and 13.5 h, respectively. Modes L11 and L12, which are also transverse mode waves, are very close to the L10 period and cannot be distinguished in the spectra. As will be seen below, by comparing data and numerical simulations, it is found that the L12 mode occurs the most often. We will call it T1 hereafter. Transverse modes were seen most clearly in the spectra in the central part of the lake basin and were often found in the eastern part. Modes higher than T1 cannot be detected with certainty because of the cut-off imposed by the SFE filter.

Numerical model results—Numerical simulations were carried out for summer stratification for an 18-h pulse of 5 m s^{-1} wind from the northeast tapering off from the center of the lake toward the eastern end. The amphidromic patterns obtained from the numerical simulation are presented in Fig. 6. Only modes L1, L3, and T1 have amplitudes that reach over 60% of the initial thermocline excursion in significant parts of the near-shore area. For mode L1, the amplitude is more than 20% higher near station 2 than near station 7.

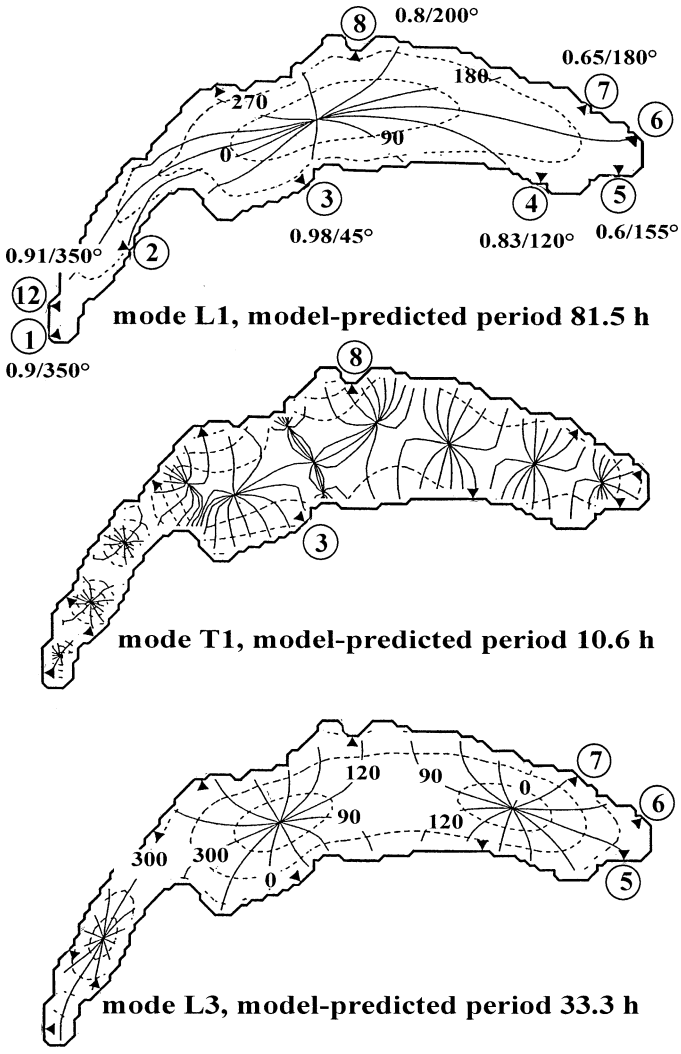

Fig. 6. Amphidromic structure and seiche periods for different seiche modes predicted by the model. Results are presented as co-range lines (dashed) in 20% steps of the maximum and cophase lines in 30° increments. Some phase angles are indicated on the cophase lines in order to indicate the sense of rotation and the relation between the cells. Seiche periods relate to the summer situation. Top: L1 mode. At each station, phase and coherence with reference to station 2 obtained from the SFE data are also indicated; for details, see text. Center: T1 mode; bottom: L3 mode.

This explains the difference in the spectral peaks of L1 (Fig. 5). The amplitude for the L3 mode is highest at the eastern end of the basin. It will be shown below that this mode is best documented in the eastern part of the lake. Mode T1 has the highest amplitudes near the shore in the center of the lake. As will be detailed below, the T1 seiches are found most often in this part of the lake.

The cotidal lines indicate that water mass displacement, produced by these three waves, progress around the whole lake basin. Modes L1 and L3 show counterclockwise rotation in all cells, which is evidence for Kelvin-type seiche modes. For mode T1, the rotation in the central part of the lake is clockwise, and in the cells toward the lake ends, it is counterclockwise. This will be discussed in detail below.

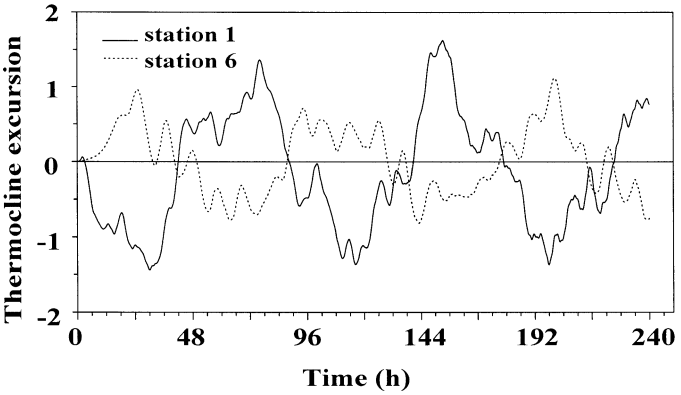

Fig. 7. Time series of thermocline excursions resulting from a numerical simulation; for details, see text. The station location is given in Fig. 6 and is indicated on each curve.

Evidence for the existence of seiche modes

Wave propagation pattern for the L1 mode and evidence for Kelvin-seiche response—Cross-spectral analysis reveals the wave propagation pattern. In each case, coherence and phase were determined between pairs of stations. In most cases, coherence was well above the 95% confidence limit. This is illustrated for the first horizontal mode L1 at end-basin stations 2 and 7 in Fig. 5.

Taking station 2 as the reference station, calculations were made for all possible station combinations. The progression of the L1 mode is presented in Fig. 6 (top panel), where corresponding coherence and phase angle are indicated for selected stations. Coherence was high for most station pairs, decreasing from west to east along the southern shore. For the stations along the northern shore, coherence increased again from east to west and became high for the stations in the narrow western basin. The phase angles calculated from the data can be compared with those predicted by the numerical model, as indicated by the corange lines. Along the southern shore, satisfactory agreement in phase angle is found. Agreement is less satisfactory on the northern shore, in particular, at the entrance to the western basin at stations 10 and 11, even though coherence is high. At the western end of the lake, agreement improved again. The cyclonic progression of this seiche is clearly established.

Numerical simulation may help explain the west–east degradation of the correlation coefficient. We forced the model with a 8-h pulse of 5 m s^{-1} wind from the northeast and simulated the topographic sheltering effect by tapering off wind velocity from the center of the lake toward the eastern end. Figure 7 shows that the modeled wave amplitude is high and the waveform is regular, almost sinusoidal, at the western end of the basin. At the eastern end, however, the amplitude is greatly reduced and the waveform is perturbed by either T1 mode seiches, to be discussed below, or nonwave effects.

Evidence for the Kelvin wave character of the L1 mode wave also comes from current and temperature recordings carried out in the northern part of the lake in 1982–1983. Figure 8 shows an extract from December to January when the lake was still weakly stratified with a thermocline at about 90 m depth. Further details can be found in Mortimer (1993). Station A1 is close to shore, whereas station A3 is further offshore (for station location, see Fig. 1). Three wind events occurred between 9 and 20 December.

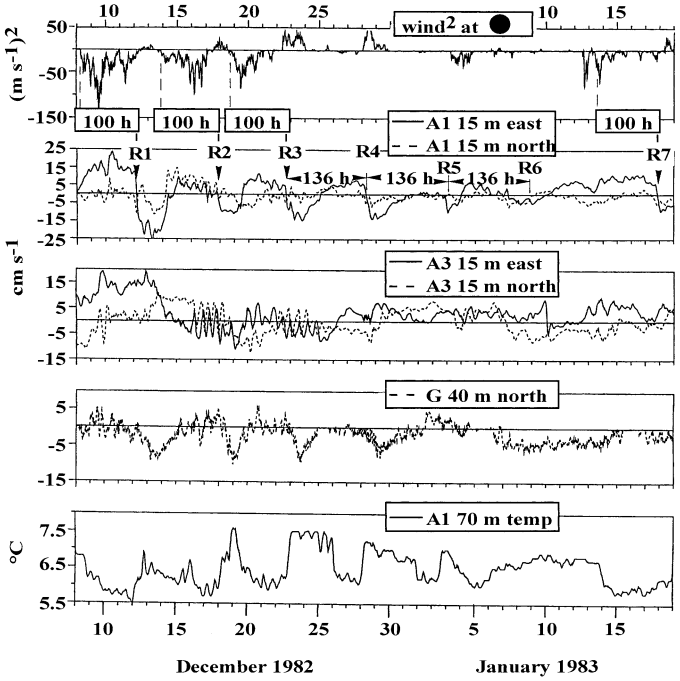

Fig. 8. Current and temperature records of fall/winter 1982–1983. For station locations, see Fig. 1.

At roughly 100 h after the start of each wind event, the currents at mooring A1 (15 m depth) suddenly reversed from east-going to west-going. Those reversals, R1, R2, R3, and R7, were each accompanied by a sudden depression of the thermocline (i.e., a sudden temperature rise) at mooring A1. Figure 8 indicates a pattern starting on the south shore that had traveled around the lake at internal seiche speed.

After the wind event R3, a free Kelvin-seiche oscillation (L1; period of 136 h) persisted for three cycles. Amplitudes of the current reversals R3–R5 and amplitudes of the associated temperature waves decrease steadily in time. At each wave passage, strong current reversals in the upper layer occurred at station A1. The temperature records again supported the Kelvin wave pattern. Pronounced signals were observed at A1.

At that time of the year, the thermocline was below the depth of the western basin. The path of a Kelvin wave should, therefore, be confined to the contour of the main basin. The signal from the L1 mode is seen in the alongshore (east–west) component at A1, whereas it appears as south-going currents at G (Fig. 8), confirming that the Kelvin wave is confined to the main basin.

Wave propagation of the T1 mode and evidence of a Poincaré-seiche response—For the only other strongly expressed mode, the transverse mode T1, coherence is only found for stations that are part of the same amphidromic cell. The results of the cross-spectral analysis for cross-basin stations 3 and 8 are given in Fig. 9.

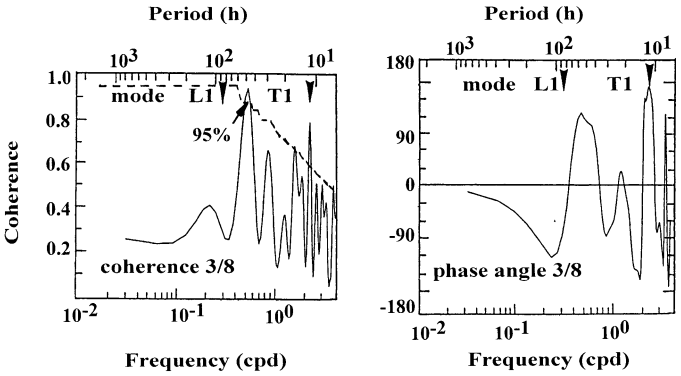

Fig. 9. The transverse mode T1 during the interval 4 June–24 August 1950: coherence and phase between stations 3 and 8. For station locations, see Fig. 6.

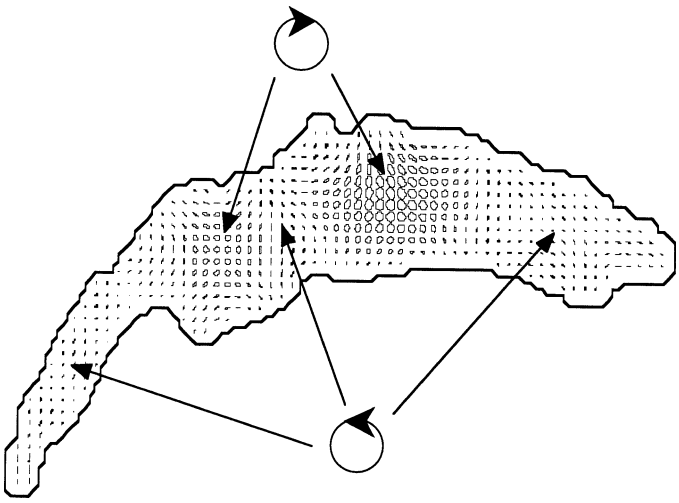

Fig. 10. Current pattern of the T1 mode calculated with the numerical model for the lower layer. The sense of rotation in the different regions of the lake is indicated.

Is this T1 mode a Poincaré wave? The effect of the Coriolis force is sufficiently strong to affect an internal seiche with near 11-h period. This is supported by results from the numerical model, which predict clockwise rotation in the amphidromic cells in the central part of the lake and counterclockwise rotation in the remaining cells. The current pattern for this T1 mode, integrated over one wave cycle, is presented in Fig. 10. In the counterclockwise-rotating cells, the current ellipses are elongated and predominantly oriented along the shore. In the clockwise-rotating cells, the current ellipses are nearly circular in the central parts of the basin, as predicted by the theory for idealized basins (Mortimer 1993). The ellipses become progressively elongated as they approach the shore or the neighboring counterclockwise rotating cells. By definition, the shore normal velocity component is zero at the shore and the transport is along the shore.

To investigate the structure of the T1 mode, current records taken during summer 2001 at station P on the central plateau (see Fig. 1 for station location) at 304 m depth, 5 m above the lake bottom using an Aanderaa RCM9 current meter were examined. This station is located in the center of the central clockwise-rotating cell (Fig. 10). Spectra (Fig. 11) of the north and the east current components, which are nearly lined up along and across the principal axis of the lake, reveal two peaks: A broad peak at the L1 frequency and a sharp peak at the T1 frequency. The L1 peak is broad because of changes in stratification characteristics over the recording interval. The energy of the east component is higher than the north component, indicating predominantly alongshore movement. The instrument was close to the center of the lake, where L1 Kelvin-wave information is strongly attenuated.

At the T1 frequency, we find a sharp peak with the energy of the two components being nearly equal. This is typical for the rotating pattern of a Poincaré wave. Indicated in this figure are also the results of the cross-spectral analysis. As discussed above, coherence is high, close to one, only for the two frequency bands of L1 and T1 waves. The phase progression changes from counterclockwise for L1 to clockwise for T1. Progressive vector diagrams (not shown here) derived from these data show the clockwise looping pattern characteristic for Poincaré waves. The same looping pattern can be found in a progressive vector diagram of the currents at A3 in Fig. 8 (not shown here). This station was located in the western clockwise-rotating cell (Fig. 10). From this analysis, the current field at the T1 frequency shows all characteristics of a Poincaré wave.

The results of the numerical simulation using the same wind field, which produced clear L1 signals at stations 1 and 6 (see Fig. 7), are given for stations 3 and 8 in Fig. 12. The Kelvin-seiche period and progression is again seen in this figure. The most striking feature is the strong, superimposed excitation of the T1 mode in this central part of the main basin.

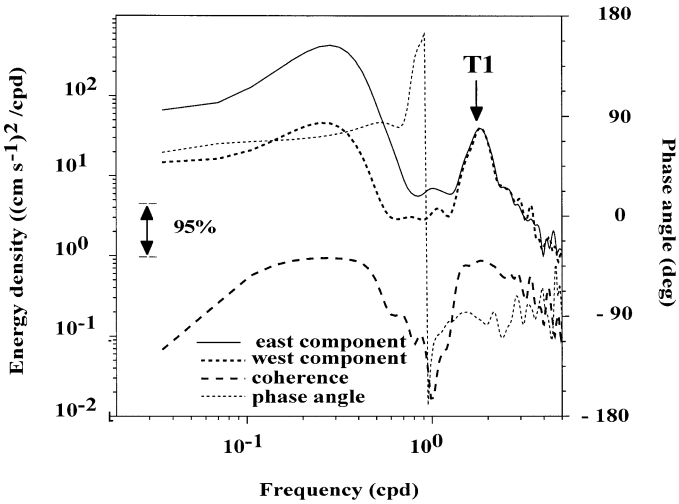

Fig. 11. Energy-density spectra of the north and east component of the currents recorded at station P (see Fig. 1 for position) during the summer 2001. Also shown are the coherence (reference to the left axis; plotted on a logarithmic scale) and the phase angle (reference to the right axis) between the two components. A positive phase angle corresponds to a counterclockwise rotation and a negative phase angle to a clockwise rotation.

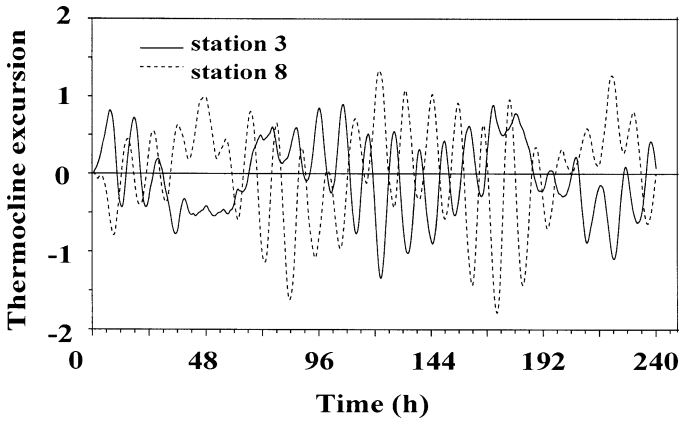

Fig. 12. Time series of thermocline excursions resulting from a numerical simulation; for details, see text. The station location is indicated for each curve.

On average, the phase angle between the two stations corresponds to a value close to 165°, which is similar to the one observed in the water level data shown in Fig. 9. However, it can be seen in Fig. 12 that the phase angle varies over time. This can be explained by recalling the results of the numerical modeling. They indicated that, in addition to mode L12 (which we named T1) presented in Figs. 6 and 10, modes L10 and L11, with somewhat different amphidromic patterns and slightly longer periods (11.5 and 10.9 h), also show Poincaré characteristics (clockwise-rotating cells) in the central part of the basin. For these two modes, the phase angle between stations 3 and 8 is closer to 120°.

The time variance of the phase angle seen in Fig. 12 indicates that, over time, the Poincaré wave is not a standing-wave pattern of only one mode. Instead, it oscillates between the three possible standing modes (L10–L12) with L12 being dominant. Due to the small difference in period between the three modes and the data-recording interval, spectral analysis of the recorded currents and the surface elevations is not capable of resolving these differences. A beat pulsation is apparently in progress (similar to those seen in Lake Michigan; Mortimer 2004), most obvious at 48 and 198 h.

Wave propagation for the L3 mode—The amphidromic pattern obtained from the numerical simulation is presented in Fig. 6. The cotidal lines indicate that water-mass displacement produced by this wave progressed around the whole lake basin. In the eastern part of the basin, several stations fall into the same cell of a mode L3 wave. The cyclonic progression is revealed by the phase angles of stations 5 and 7 with respect to the central station 6 (Fig. 13). Thus, the L3 seiche has Kelvin-wave characteristics.

The excitation of the L3 mode is observed to be particularly strong during fall at the eastern end of the basin (Fig. 13). We forced the lake model (with fall stratification) by a 5-m s^{-1} wind for 12 h from the southeast, tapering off to zero toward the center of the lake. This simulates the effects of valley wind, documented for the Rhone valley (Lemmin and D'Adamo 1996). The time series of thermocline excursions (Fig. 14) shows undulations with a period of about 50 h, which is the L3 period disclosed by spectral analysis of

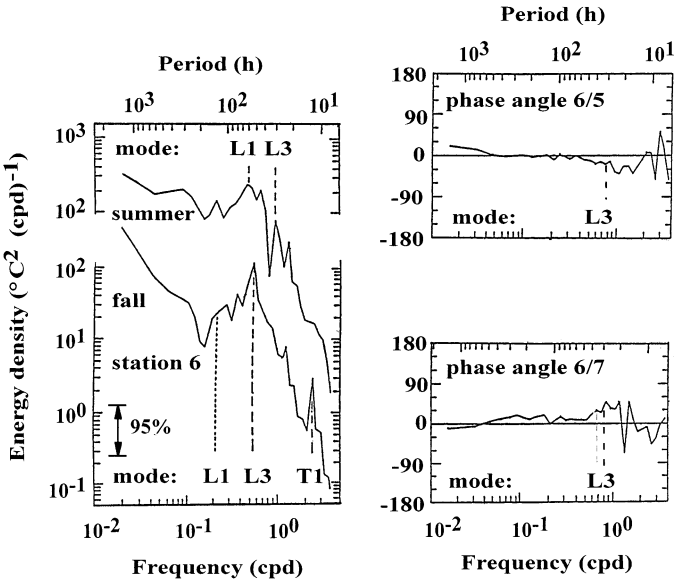

Fig. 13. Left-hand panel: Spectra of SFE surface-level fluctuations at station 6, upper spectrum for the summer interval, lower spectrum for the fall period (note the scale break in the energy scale). Also shown (right-hand panels; for the summer period) are the phase-angle diagrams for the station pairs 6/5 and 6/7, indicating cyclonic progression of mode L3 (eastern amphidrome; see Fig. 6).

the SFE data during the fall (Fig. 13). It is also evident from Figure 14 that an L3-mode pattern is only established after the excitation has passed through the whole basin.

The excitation of seiche modes by wind

Mode excitations produced by model winds—The numerical model was used to explore why only certain modes are excited. Winds of equal strength and duration, but from different directions (south, west, southwest), were applied to the model lake and the responding mode structures were analyzed. For the L1 mode, highest amplitudes were produced by winds from the west and southwest. These are the

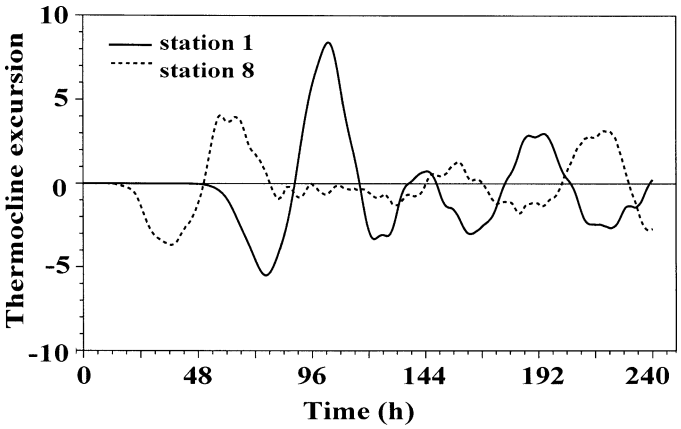

Fig. 14. Time series of thermocline excursions at different stations resulting from a numerical simulation; for details, see text. The station location (see Fig. 6) is indicated on the curves.

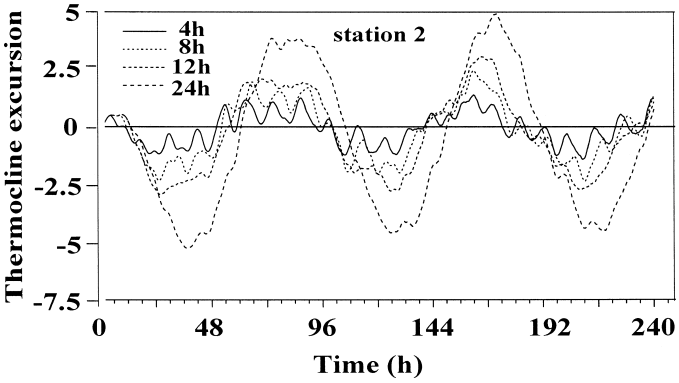

Fig. 15. Thermocline excursions at station 2 resulting from a numerical simulation for different wind-event durations; for details, see text. The wind-event duration is indicated for each curve.

wind directions that occur most often over the whole basin or a significant part of it. Those winds, however, do not excite a second mode of significant amplitude. Only winds from the south can generate L2 mode waves with noticeable amplitude. However, sheltering by the Alps along the southern shore of the lake rules out strong, persistent wind forcing from that direction (Fig. 1). Winds from the south may come down the narrow valley, which cuts into the Alps behind station 3, thus exposing a limited area of the central part of the lake basin. We found high coherence between stations 3 and 8 in the central basin (Fig. 9) at the L2 period but not with other stations.

The response of the L3 mode is highest for winds from the west and is comparable with that for the L1 mode. Modes four to nine are excited by all winds but have generally very low amplitudes. The T1 mode is again excited by all observed winds and it has an amplitude that is comparable with that found for the L1 and L3 modes. From this analysis, it follows that typical winds over the lake can only excite those three modes with sufficient amplitude. This conclusion and the model prediction are supported by the observations.

Coupling between different mode excitation—We used the numerical model to explore the possibility of such coupling. When comparing two stations (3 and 8) in the center of the lake (Fig. 12) subjected to the same wind regime, the results were as follows: The T1 mode was strongly excited and out-of-phase on the two sides, whereas the dominant L1 mode was excited at the same time and out-of-phase at the basin ends. Wind events from the southwest show the same coupling between the L1 and T1 modes.

In a second case, a wind stress was again applied over the western 60% of the basin, tapering off to the east. In this case, the duration of the wind pulse was changed from 4 h to 24 h in 4-h steps. Such variability of the wind field has been observed over the lake (Lemmin and D'Adamo 1996). With increasing duration of the wind pulse, the signal (Fig. 15) progressively took the form of a smooth sinusoidal (linear) Kelvin seiche. With an increase of wind duration, progressively less direct contribution to T1 seiche excitation was observed. However, when wind during the 24-h forcing was varied in 4-h steps around a 5-m s^{-1} mean with constant direction, T1 mode waves were again excited, together with the smooth L1 Kelvin seiche (not shown here).

From the different simulations, it appears that the same wind sets up both L1 and T1 modes. Short pulses and short-term variability of the wind field favor the development of T1 seiches, whereas the excitation of Kelvin seiches is weak. The Kelvin-seiche response will dominate with winds lasting 18 h or more.

Discussion

Coherence and phase angle patterns, evident in the present study, demonstrate that basinwide modes do occur. We do not find support for the hypothesis put forth by Bohle-Carbonell and van Senden (1990), who suggested that basinwide modes do not exist in the Lake of Geneva. The rates of frictional damping, observed in the measurements (Fig. 8) and applied in numerical simulations (not shown here), may explain why their particular statistical net caught so few basin modes.

The finding that we could reliably identify only Kelvin modes L1 and L3 and Poincaré mode T1 in the Lake of Geneva suggests that, in large and small lakes, different factors control the generation of internal seiches. In large lakes, the excitation of selected modes is direct and can be linked to the structure (stress distribution and curl; Lemmin and D'Adamo 1996) of the wind field. Topographic sheltering also plays an important role. This is different in small lakes, where a more homogeneous wind field over the lake can be expected, and higher modes are generated in a continuous mode sequence when the seiches are reflected at the ends of the basin (Lemmin 1987). Seiches of the second vertical mode, described in detail in a small lake (Lemmin 1987), were not found in the Lake of Geneva. Therefore, a two-layer model is sufficient for the interpretation of the internal seiche dynamics.

Observations and numerical simulation indicate that, most of the time, internal seiches are excited by wind events that have much shorter duration than the seiche periods. It is further seen that, the shorter the wind pulse, the more front-like the initial Kelvin-seiche response will be in the lake. Frontal steepness of internal seiches has been observed after strong wind pulses in lakes of all sizes (Mortimer 1955; Thorpe et al. 1972; Farmer 1978; Hamblin 1978; Lemmin 1987). The observed fronts in the Lake of Geneva evolve into regular seiches as time passes. This justifies the use of a linear model for the determination of seiche characteristics. We did not observe the same frontal steepening for the Poincaré seiches.

The passage of the large-amplitude, shore-hugging Kelvin seiches produce thermocline displacements over bottom slopes, sometimes extending laterally 100 m or more offshore (Thorpe et al. 1996). This creates strong bottom shear associated with high turbulent energy-dissipation rates and the potential for sediment resuspension.

The importance of internal seiches in lake dynamics in the generation of short progressive internal waves during the passage of an internal seiche has been demonstrated (Thorpe et al. 1996). Those authors suggest several ways in which

Kelvin and short-internal waves may be linked and energy transferred from internal seiches to short internal waves. Horn et al. (2002) confirm the suggestion, and Saggio and Imberger (1998) have provided evidence of such a link in Lake Biwa. This constitutes another process by which turbulence in the benthic boundary layer is produced. Imberger (1998) has noted the importance of internal wave–slope interaction in determining the particle-flux path.

The present detailed study of internal lake dynamics was mainly based on water-level records and has confirmed the potential value of these records, which was initially demonstrated by Mortimer (1963). Easily installed and maintained, water-level recorders can be operated year-round, without interfering with other activities on the lake, such as commercial drift netting, which precludes the use of midwater moorings. As an alternative, near-bottom temperature recorders may be employed (Thorpe and Lemmin 1999).

The coupling of the analysis of different types of field data with numerical modeling has proven to be a powerful approach to the understanding of the phenomena observed in the Lake of Geneva. Although we have used a relatively simple model in hindcasting mode, it provides a satisfactory interpretation of the observed motions and will be useful in designing strategies for future measurement campaigns concerning internal seiches.

References

BÄUERLE, E. 1985. Internal free oscillations in the Lake of Geneva. Annales Geophysicae **3:** 199–206.

BOHLE-CARBONELL, M. 1986. Currents in Lake Geneva. Limnol. Oceanogr. **31:** 1255–1266.

———, AND D. VAN SENDEN. 1990. On internal seiches and noisy current fields—theoretical concepts versus observations, p. 81–105. *In* M. Tilzer and C. Seruya [eds.], Large lakes. Springer.

CALOI, P., M. MIGANI, AND G. PANNOCCHIA. 1961. Ancora sulle onde interne del lago di Bracciano e sui fenomeni ad esse collegati. Ann. Geofisica, Roma **14:** 345–355.

FARMER, D. M. 1978. Observations of long nonlinear internal waves in a lake. J. Phys. Oceanogr. **8:** 63–73.

FOREL, F. A. 1895. Le Léman: Monographie Limnologique. Rouge. Lausanne.

HAMBLIN, P. R. 1978. Internal Kelvin waves in a fjord lake. J. Geophys. Res. **83:** 2409–2419.

HORN, D. A., J. IMBERGER, G. N. IVEY, AND L. G. REDEKOPP. 2002. A weakly nonlinear model of long internal waves in closed basins. J. Fluid Mech., **467:** 269–287.

IMBERGER, J. 1998. Flux paths in a stratified lake: a review, p. 1–17. *In* J. Imberger [ed.], Physical processes in lakes and oceans. Coastal and Estuarine Studies, 54. Amer. Geophys. Un.

KANARI, S. 1975. The long-period internal waves in Lake Biwa. Limnol. Oceanogr. **20:** 544–553.

———. 1984. Internal waves and seiches, p. 185–235. *In* S. Horie [ed.], Lake Biwa. Junk.

LEMMIN, U. 1987. The structure and dynamics of internal waves in Baldeggersee. Limnol. Oceanogr. **32:** 43–61.

———, AND N. D'ADAMO. 1996. Summertime winds and direct cyclonic circulation: Observations from Lake Geneva. Ann. Geophysicae **14:** 1207–1220.

MORTIMER, C. H. 1953. The resonant response of stratified lakes to wind. Schweiz. Z. Hydrol. **15:** 94–151.

———. 1955. Some effects of earth rotation on water movements in stratified lakes. Verh. Int. Ver. Limnol. **12:** 66–77.

———. 1963. Frontiers in physical limnology with particular reference to long waves in rotating basins. Proc. 5th Conf. Great Lakes Res. Div., Univ. Michigan, 9–42.

———. 1993. Long internal waves in lakes: Review of a century of research. Special report, 42, Univ. Wisconsin–Milwaukee, Center for Great Lakes Studies.

———. 2004. Lake Michigan in motion: Responses of an inland sea to weather, earth-spin and human activities. University of Wisconsin Press.

PLATZMAN, G. 1971. Ocean tides and related waves. Amer. Math. Soc. Lectures Appl. Math. **14:** 239–291.

SAGGIO, A., AND J. IMBERGER. 1998. Internal wave weather in a stratified lake. Limnol. Oceanogr. **43:** 1780–1795.

SERVICE FÉDÉRAL DES EAUX; SFE. 1954. Les dénivellations du lac Léman. Département fédéral des postes et des chemins de fer. Report, maps, figures.

SIRKES, Z. 1987. Surface manifestations of internal oscillations in a highly saline lake (the Dead Sea). Limnol. Oceanogr. **32:** 76–82.

THORPE, S. A., A. J. HALL, AND I. CROFTS. 1972. The internal surge in Loch Ness. Nature. **237:** 96–98.

———, K. J. KEEN, R. JIANG, AND U. LEMMIN. 1996. High frequency internal waves in Lake Geneva. Phil. Trans. Roy. Soc. London A. **354:** 237–257.

———, AND U. LEMMIN. 1999. Internal waves and temperature fronts on slopes. Ann. Geophysicae **17:** 1227–1234.

WEDDERBURN, E. M. 1912. Temperature observations in Loch Earn, with a further contribution to the hydrodynamical theory of the temperature seiche. Trans. Roy. Soc. Edinburgh. **48:** 629–695.

Received: 3 November 2003
Accepted: 17 June 2004
Amended: 10 August 2004